PAPER

Check for updates

Synthesis of core–shell ZIF-67@Co-MOF-74 catalyst with controllable shell thickness and enhanced photocatalytic activity for visible light-driven water oxidation†

Changyan Guo, Jia Guo, Yonghong Zhang, [iD]* Di Wang, Li Zhang, Yuan Guo, Wenlan Ma and Jide Wang [iD]*

In this paper, a core–shell ZIF-67@Co-MOF-74 catalyst was synthesized by coating 2,5-dihydroxyterephthalic acid (DHTP) molecules on the surface of ZIF-67 crystals *via* the ligand exchange method. Notably, the ZIF-67@Co-MOF-74 catalyst with shell thicknesses of 10 nm, 25 nm and 50 nm can be further obtained by adjusting the mass ratio of ZIF-67 and DHTP. Compared to individual ZIF-67 or Co-MOF-74 catalyst, the as-prepared core–shell MOF catalyst exhibited enhanced photocatalytic activities for light-driven water oxidation reaction. Furthermore, the content of oxygen evolution by water splitting increased gradually with the increase in shell thickness. The formation of crystal defects and the uncoordinated hydroxyl and carboxyl groups on the surface of core–shell MOFs facilitated the exposure of the metal catalytic center and the adsorption of water molecules through hydrogen bonding interactions to react with the catalytic active center effectively. In addition, the photogenerated holes and electrons could be excellently separated and rapidly transferred at the interface of ZIF-67 (core) and Co-MOF-74 (shell), resulting in effective increase in the interfacial charge transfer rate. Furthermore, this simple and novel method is also applicable to three other carboxylic acid ligands, which implies that it may be a general method that can be extended to other ligands for fabricating different core–shell ZIF-67@MOF crystals.

Introduction

As a clean, green and renewable energy, solar energy has attracted worldwide attention.[1,2] Hydrogen production *via* a photocatalytic water splitting process assisted by solar energy is an efficient approach to address the energy crisis.[3,4] The overall water splitting process involves two half-reactions: proton reduction (HER, evolution of H_2) and water oxidation (OER, evolution of O_2).[5,6] OER is considered as a hindrance in the water splitting reaction, which is required for the transfer of $4e^-$ and $4H^+$ in one catalytic cycle. Due to the slow OER kinetics and a greater natural overpotential ($(2H_2O \rightarrow 4H^+ + 4e^- + O_2)$ $E_0 = -1.23$ eV), it is difficult to conduct the water oxidation process in the absence of a catalyst.[7,8] However, a valuable catalyst can effectively lower the energy barriers and may accelerate the reaction rates. Therefore, it is necessary to develop an efficient and stable photocatalyst for converting solar energy into chemical energy.[9]

Key Laboratory of Oil and Gas Fine Chemicals, Ministry of Education & Xinjiang Uygur Autonomous Region, College of Chemistry and Chemical Engineering, Xinjiang University, Urumqi 830046, P. R. China. E-mail: zhzhzyh@126.com, awangjd@sina.cn
† Electronic supplementary information (ESI) available. See DOI: 10.1039/c8ce01266k

At present, light-driven water oxidation catalysts reported in the literature can be divided into homogeneous catalysts and heterogeneous catalysts.[10–16] Although homogeneous catalysts have higher reactivity due to easy combination with the photosensitizer $[Ru^{III}(bpy)_3]^{3+}$ in the form of a complex, they also have some drawbacks such as poor stability, depletion and rapid inactivation of metal ions. Compared to homogeneous catalysts, heterogeneous catalysts often show good stability, diverse morphological structures and recycling performance. From recent literature reports[17,18] and previous studies of our research group,[19–21] Co-based heterogeneous catalysts have proven to be promising catalysts for the water oxidation reaction. Since the oxidation process of water molecules is performed on the surface of the catalyst, the synthesis of catalysts with hierarchical structures with large specific surface areas and ultra-small nanometer sizes can provide relatively more active sites to improve their catalytic activity. Also, a pore-rich structure facilitates rapid transmission of electrons and diffusion of water molecules. Thus, the development of low-cost Co-based heterogeneous photocatalysts with large specific surface area and pore-rich structure is critical for the light-driven water oxidation reaction.

Metal–organic frameworks (MOFs) are a special type of porous materials self-assembled from metal ions (or metal

clusters) with multi-dentate organic ligands *via* coordination bonds.[22] Compared with mesoporous silica, zeolite and activated carbon, MOFs have unique topological structures, ultrahigh surface areas, different highly ordered pore structures, tailorable molecular cavities, and feasible post-synthetic modifications.[23,24] Additionally, uncoordinated metal nodes, guest molecules loaded in the pores, structural defects in the crystal and bridging ligands can all act as catalytic active sites.[25,26] Various MOFs have been successfully used as effective catalysts for water oxidation reaction.[27–30] To further improve the catalytic performance of MOF catalysts, researchers have found that the existence of defects and vacancies can effectively improve the photocatalytic performance.[31–33] The core–shell catalyst not only maintains the excellent performance of both core and shell materials, but also effectively overcomes the disadvantages of single materials, exhibiting properties that are different from those of single-component cores or shells of MOFs.[34] Moreover, there is a clear interface between the core and shell of the core–shell structure, which is more conducive to electron transport and can effectively increase the interfacial charge transfer rate.[19,35–37]

Herein, we report an efficient and general method for the synthesis of ZIF-67@MOFs (MOFs = Co-MOF-74, Co-BDC, Co-NH₂BDC and Co-BTC) core–shell catalysts by the ligand exchange method. In addition, ZIF-67@Co-MOF-74 catalysts with controllable shell thicknesses can be easily prepared through adjusting the mass ratio of DHTP and ZIF-67. The photocatalytic results show that ZIF-67@Co-MOF-74 core–shell catalysts exhibit higher catalytic activity than pure ZIF-67 and pure Co-MOF-74 catalysts for visible light-driven water oxidation.

Results and discussion

Synthesis of core–shell ZIF-67@Co-MOF-74 with controllable shell thicknesses

The core–shell ZIF-67@Co-MOF-74 catalyst was synthesized by exchanging ligands on the surface of ZIF-67 with DHTP molecules. DHTP molecules have stronger coordination ability than 2-MI; thus, when they were added to the dispersion of ZIF-67, DHTP molecules could compete with 2-MI on the surface of ZIF-67 to coordinate with cobalt, and a crystal of Co-MOF-74 was formed on the surface of ZIF-67 to afford a ZIF-67@Co-MOF-74 core–shell structure (Fig. 1).

In addition, core–shell MOFs with controllable shell thicknesses can also be prepared by altering the mass ratio of ZIF-
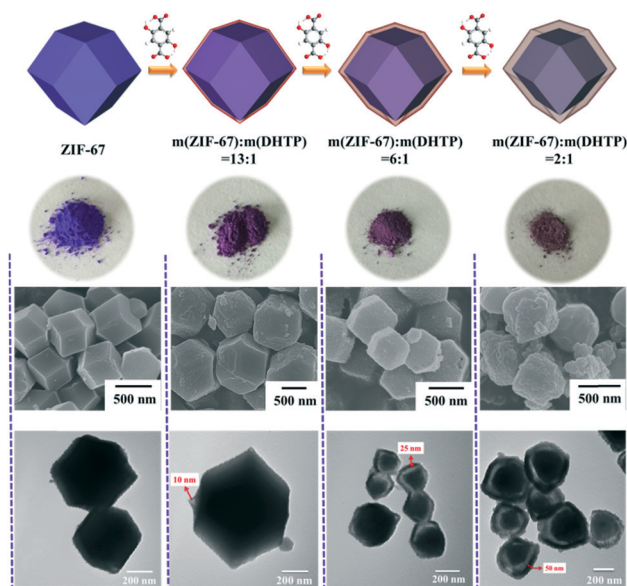

Fig. 2 A simplified figure of the synthesis of core–shell ZIF-67@Co-MOF-74 catalysts with controllable shell thickness and their SEM/TEM images.

67 crystals and DHTP. It can be seen from Fig. 2 that as the DHTP concentration increases, the color of the resulting ZIF-67@Co-MOF-74 crystal gradually changes from the original purple of ZIF-67 to purple-gray. The SEM results show that ZIF-67 exhibits dodecahedron morphology and the crystal size is about 500 nm. The formation of ZIF-67@Co-MOF-74 core–shell structure does not significantly affect the morphology and size of the crystal except that the surface of the crystal is no longer smooth, resulting in many crystal defects. In addition, it can also be seen from the figure that a layer of crystal is formed on the surface of ZIF-67. The TEM results further confirmed the formation of ZIF-67@Co-MOF-74 crystal, and it was found that core–shell MOFs with different shell thicknesses can be prepared by increasing the concentrations of DHTP. When m(ZIF-67) : m(DHTP) was 13 : 1, only a thin layer of Co-MOF-74 crystal with a thickness of about 10 nm could be formed on the surface of ZIF-67. As the mass ratio decreased to 6 : 1, the thickness of the shell increased to 25 nm. When the mass ratio further decreased to 2 : 1, the
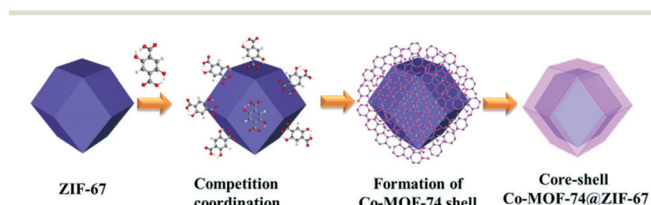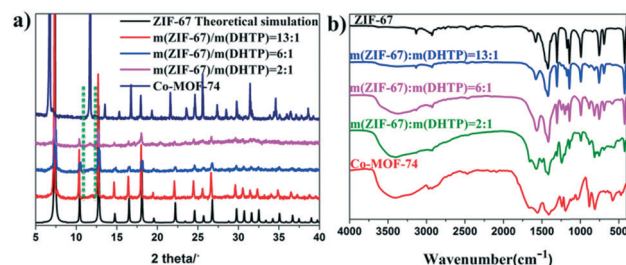

Fig. 3 a: PXRD patterns of ZIF-67, Co-MOF-74 and ZIF-67@Co-MOF-74 crystals with different shell thicknesses; b: FTIR spectra of ZIF-67, Co-MOF-74 and ZIF-67@Co-MOF-74 crystals with different shell thicknesses.

Fig. 1 The synthetic route of ZIF-67@Co-MOF-74 crystal.

shell thickness reached 50 nm. However, with further decrease of ZIF-67/DHTP molar ratio, the original dodecahedron crystal of ZIF-67 completely disintegrated to form an amorphous bulk crystal.

PXRD and IR analysis

To confirm that the shell formed on the surface of ZIF-67 was Co-MOF-74 crystal, PXRD and IR of ZIF-67, Co-MOF-74 and ZIF-67@Co-MOF-74 crystals with different shell thicknesses were studied. According to the XRD results, ZIF-67 and Co-MOF-74 have their own unique crystal diffraction peaks.[38,39] The core–shell ZIF-67@Co-MOF-74 mainly exhibits diffraction peaks of ZIF-67, indicating that the as-prepared core–shell MOFs are mainly ZIF-67. However, the characteristic diffraction peak of Co-MOF-74 located at 11.9° appeared in the PXRD diffraction pattern of the core–shell MOFs, and the peak intensity gradually increased with the increase in shell thickness. This result confirmed that the shell formed on the surface of ZIF-67 exhibits a small amount of Co-MOF-74 crystals and preliminarily determines the formation of ZIF-67@Co-MOF-74 core–shell structure. Subsequently, a comparative IR analysis was also performed on these materials. From Fig. 3, it can be seen that an unsaturated C–H stretching vibration peak located at 3415 cm^{-1} appeared in the core–shell MOFs, which was assigned to the C–H stretching vibration of benzene ring of DHTP, indicating that DHTP was coordinated on the surface of ZIF-67 crystal by the ligand exchange method. In addition, as the shell thickness increased, the absorption peak of the core–shell MOFs gradually shifted from the characteristic peak of ZIF-67 to that of Co-MOF-74, further confirming the formation of core–shell ZIF-67@Co-MOF-74.

Elemental distribution analysis

As can be seen from the EDS mapping results (Fig. 4), the corresponding metal elements are evenly distributed on the whole surface of ZIF-67 and core–shell ZIF-67@Co-MOF-74 crystals. Notably, the oxygen content on the crystal surface increased and the nitrogen content decreased, which further confirmed that the 2-MI ligand on the surface of ZIF-67 was replaced by DHTP molecule to form core–shell ZIF-67@Co-MOF-74 crystals.
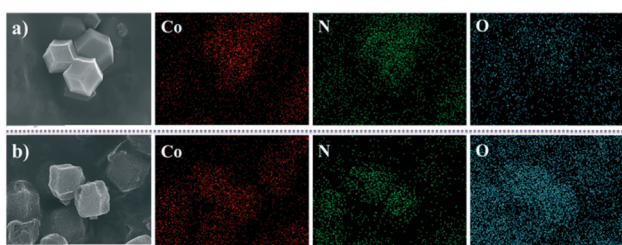
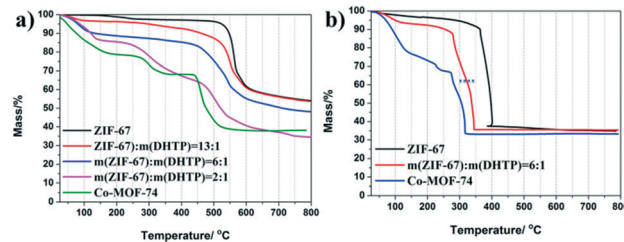Fig. 4 a: EDS mapping images of ZIF-67; b: EDS mapping images of ZIF-67@Co-MOF-74 (6 : 1).

Fig. 5 a: TGA of ZIF-67, Co-MOF-74 and ZIF-67@Co-MOF-74 crystals with different shell thicknesses under argon atmosphere; b: TGA spectra of ZIF-67, Co-MOF-74 and ZIF-67@Co-MOF-74 crystals with different shell thicknesses under air atmosphere.

Thermal stability analysis

Subsequently, the thermal stability of the prepared core–shell MOFs was compared with those of ZIF-67 and Co-MOF-74 under an argon atmosphere and an air atmosphere, respectively. As shown in Fig. 5a, the ZIF-67 material exhibited a minor weight loss before 150 °C under an argon atmosphere, indicating that almost all of the free water is present on the surface and the pores of the material are desorbed. The material quickly lost about 30% of mass when heated to 500 °C, and this weight loss process basically ended at 600 °C. It indicated that the ZIF-67 material was stable under 500 °C, and the structure of the material could collapse when the temperature reached 500 °C.[40] For Co-MOF-74, the first weight loss around 200 °C was caused by the removal of solvent molecules adsorbed in the pores, and the second weight loss up to 400 °C can be ascribed to the removal of guest molecules.[39] The final collapse for Co-MOF-74 occurred at lower temperatures compared to that for ZIF-67. Core–shell ZIF-67@Co-MOF-74 exhibited a certain weight loss before the structure collapsed, contributed by guest molecules. The core–shell MOFs prepared with a mass ratio of 2 : 1 exhibited a significant weight loss between 250 and 400 °C, which is due to the decomposition of the DHTP molecules on the surface of the crystal. This part of the
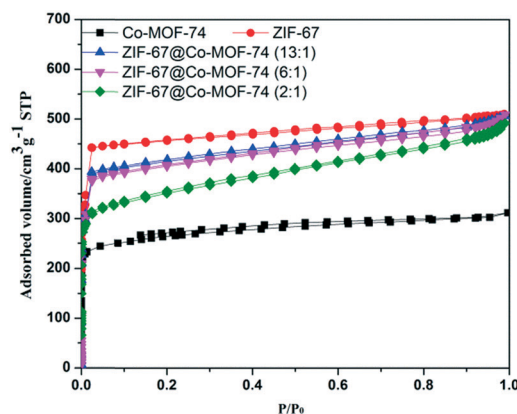
Fig. 6 N$_2$ adsorption/desorption isotherms of Co-MOF-74, ZIF-67 and core–shell ZIF-67@Co-MOF-74 catalysts with different shell thicknesses.
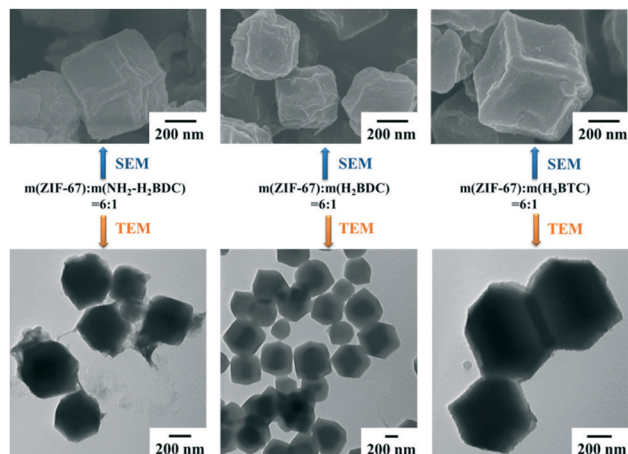
Fig. 7 SEM and TEM images of ZIF-67@Co-BDC, ZIF-67@Co-NH$_2$-BDC and ZIF-67@Co-BTC crystals.

Fig. 9 Schematic representation of the proposed mechanism for visible light-driven OER by core–shell ZIF-67@Co-MOF-74.

DHTP molecule may not be involved in the construction of the crystal structure but is only adsorbed onto the crystal surface by weak coordination.

A similar phenomenon was also found in the results obtained from air atmosphere. As can be seen in Fig. 5b, ZIF-67 quickly loses weight after 365 °C and 35% of Co$_3$O$_4$ is obtained as the only product. Co-MOF-74 showed weight loss in the range from 280 °C to 300 °C, which can be ascribed to the collapse of the crystal structure; the final decomposition for ZIF-67@Co-MOF-74 prepared at a mass ratio of 6:1 appeared at a higher temperature. It can also be seen from the figure that the TGA pattern of core–shell MOFs between 280 and 350 °C comprises two-step weight reduction. The first stage is before 320 °C, which is the decomposition of the crystal structure of the shell Co-MOF-74. The rapid weight loss between 320 and 350 °C can be due to the decomposi-
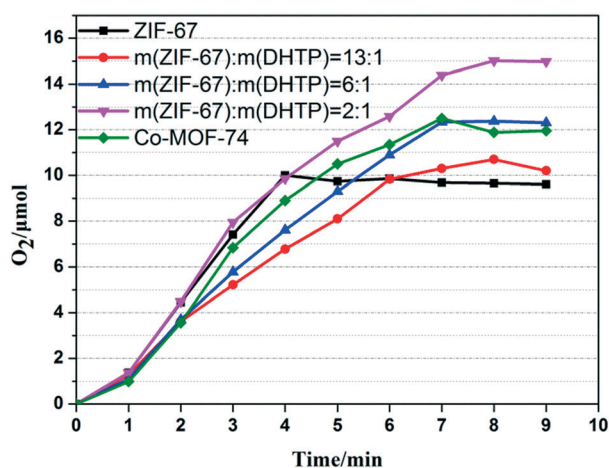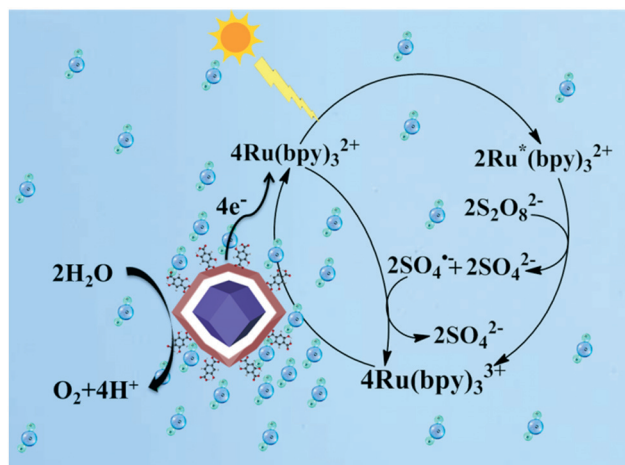

Fig. 8 Kinetics of O$_2$ evolution of the photocatalytic system with ZIF-67, Co-MOF-74 and core–shell ZIF-67@Co-MOF-74 with different shell thicknesses as catalysts. Conditions: Xe lamp ($\lambda \geq$ 420 nm, 26.4 mW cm^{-2}); catalyst (1 mg); 5.0 mM Na$_2$S$_2$O$_8$; 80 mM sodium borate buffer (initial pH, 9.0) and 1.0 mM [Ru(bpy)$_3$](ClO$_4$)$_2$; total reaction volume: 10 mL.

tion of the ZIF-67 core. This result further proves the formation of core–shell MOFs. In addition, although the stability of core–shell ZIF-67@Co-MOF-74 is slightly lower than that of ZIF-67, the content of metal cobalt in core–shell MOFs is not reduced, and 35% of metal oxides is obtained.

N$_2$ adsorption/desorption isotherms

ZIF-67, Co-MOF-74 and core–shell ZIF-67@Co-MOF-74 catalysts with different shell thicknesses were tested for nitrogen adsorption. The N$_2$ adsorption/desorption isotherms of the catalysts were characterized at 77 K, and the isotherms of the five types of MOFs were type I according to the IUPAC classification of isotherm shapes (Fig. 6).[41] Table S1† summarizes the values estimated from the isotherms. It can be found that Co-MOF-74 exhibited a specific surface area of 882 m^2 g^{-1}, and the specific surface area of ZIF-67 reached 2129 m^2 g^{-1}. For ZIF-67@Co-MOF-74, with the increase in shell thickness, both the specific surface area and pore size (Fig. S1†) gradually decreased. This further demonstrated the formation of core–shell MOFs with different shell thicknesses.

Synthesis of other three core–shell ZIF-67@MOFs

In addition to synthesizing core–shell ZIF-67@Co-MOF-74 using DHTP molecules as a competitive coordination reagent, it was also found that ligand exchange can occur on the surface of ZIF-67 while using H$_2$BDC, NH$_2$-H$_2$BDC, and H$_3$BTC molecules as the competitive ligands. It can be seen from Fig. 7 that different MOF shells can be formed on the surface of ZIF-67 by the ligand exchange strategy. The crystal morphology was slightly damaged during the formation of core–shell MOFs, but no significant changes in crystal size occurred. This result shows that preparation of core–shell MOFs by ligand exchange methods does not increase the size of the resulting crystals, whereas the epitaxial growth strategy generally results in an increase in the crystal size. In addition, the formation of different core–shell MOFs also

indicated that this method is suitable for different carboxylic acid organic ligands, and it can be extended to other ligands to prepare different core–shell ZIF-67@MOF crystals.

Water oxidation kinetics and mechanistic analysis

The catalytic performances of ZIF-67, Co-MOF-74 and core–shell MOFs were evaluated by the light-driven water oxidation reaction (Fig. 8). In the boric acid buffer solution of pH = 9.0, after 4 minutes of visible light irradiation, the amount of evolved O_2 catalyzed by ZIF-67 was 9.8 µmol. After using Co-MOF-74 as a catalyst, the amount of evolved O_2 could reach 11.8 µmol after 7 minutes of visible light irradiation. Under the same reaction conditions, the oxygen production of core–shell MOFs reached the maximum after 8 minutes of visible light irradiation, and the amount of evolved O_2 increased with the growth of shell thickness. When the thickness of the MOF shell was 50 nm, the amount of oxygen evolution production could reach up to 15 µmol. However, after prolonging the irradiation time of the reaction, the oxygen production did not continue to increase. Our previous studies have shown that this is due to change in the pH of the reaction solution. By screening the sodium persulfate concentration, the pH value and the amount of core–shell MOF catalyst (m(ZIF-67) : m(DHTP) = 2 : 1) (Fig. S2–S4†), the O_2 evolution amount could reach 122 µmol, and the quantum yield (QY) was 11.3%, which was higher than those of ZIF-67 (10.1%) and Co-MOF-74 (10.3%). The AQE_{BET} values for ZIF-67, ZIF-67@Co-MOF-74 (2 : 1) and Co-MOF-74 were 0.5%, 0.9% and 1.1%, respectively, after normalizing QY with BET surface area (AQE_{BET} = apparent quantum yield/BET value of sample × 100). In addition, the core–shell catalyst can be stably recycled 5 times without significant reduction in catalytic performance (Fig. S5†), and the XRD result of the reused ZIF-67@Co-MOF-74 (2 : 1) catalyst (Fig. S6†) revealed that core–shell MOFs have good reusability and stability.

Based on the literature reports[10,42,43] and our above-mentioned experimental results, the catalytic mechanism of core–shell ZIF-67@Co-MOF-74 in the visible light-driven water oxidation is demonstrated in Fig. 9. In a photoinduced sacrificial system consisting of $[Ru(bpy)_3]^{2+}$ (photosensitizer) and $Na_2S_2O_8$ (sacrificial reagent), two equivalent orange $[Ru(bpy)_3]^{2+}$ species can be oxidized to $[Ru(bpy)_3]^{2+*}$ by absorbing photons under the irradiation of visible light. Subsequently, the electrons are transferred from $[Ru(bpy)_3]^{2+*}$ to $S_2O_8^{2-}$ due to the quenching effect of $Na_2S_2O_8$ to generate $[Ru(bpy)_3]^{3+}$, SO_4^{2-} and $SO_4^{•-}$ radical anions. Simultaneously, two equivalent $[Ru(bpy)_3]^{2+}$ species can be directly oxidized to form $[Ru(bpy)_3]^{3+}$ by $SO_4^{•-}$ radical anions, which shows a higher electrode potential. Finally, water is oxidized by $[Ru(bpy)_3]^{3+}$ and form O_2 in the present of ZIF-67@Co-MOF-74 catalyst.

In photocatalytic cycles, the electron transfer rate from the catalyst to the oxidized photosensitizer has a profound effect on the overall efficiency of oxygen production.[41] For core–shell ZIF-67@Co-MOF-74, the improvement in performance may be contributed by the following three reasons: first, the surface of the core–shell MOFs formed by the ligand exchange method is no longer smooth, and many crystal defects are formed, which facilitates the exposure of the metal catalytic center and its sufficient contact with the reaction system. Second, since DHTP molecule having hydroxyl group and carboxyl group is introduced on the surface of the core–shell crystal, it is advantageous for adsorbing water molecules and causing more water molecules to split on the surface or pores of the catalyst to generate oxygen. Finally, the interface of core–shell MOFs is more conducive for rapid electron transport, which is helpful for the effective separation of electrons and holes to sufficiently inhibit charge recombination,[44] resulting in effective increase in the interfacial charge transfer rate.

Conclusions

In summary, for the first time, ZIF-67@Co-MOF-74 catalysts with controllable shell thicknesses were prepared through a simple and novel ligand exchange method. Since DHTP has stronger coordinating ability than 2-MI, it competes with 2-MI to coordinate with metal cobalt, forming a layer of Co-MOF-74 crystals on the surface of ZIF-67 to obtain core–shell Co-MOF-74@ZIF-67. The core–shell MOFs show enhanced catalytic performance for the water oxidation reaction compared to individual ZIF-67 or Co-MOF-74. This method can also be applied to other three carboxylic acid ligands, which implies that it may be a universal method and can be extended to other ligands to prepare different core–shell ZIF-67@MOF crystals.

Experimental

Synthetic procedure for ZIF-67

ZIF-67 was prepared according to a modified literature method.[33] Briefly, 2.910 g (10 mmol) cobalt nitrate hexahydrate was dissolved in methanol solution (200 mL) and then, 3.284 g 2-methylimidazole (40 mmol) was dissolved in the methanol solution (200 mL). The mixture solution was stirred at room temperature for 0.5 h and aged at room temperature for 24 h. The crystals were collected by centrifugation, washed several times with methanol, and finally dried at 60 °C under vacuum.

Synthetic procedure for ZIF-67@Co-MOF-74

ZIF-67@Co-MOF-74 was synthesized according to the following procedure. Briefly, ZIF-67 (0.3 g) was dispersed in 200 mL of methanol and then, a methanol solution of dissolved DHTP [0.02 g (m(ZIF-67) : m(DHTP) = 13 : 1); 0.05 g (m(ZIF-67) : m(DHTP) = 6 : 1); 0.15 g (m(ZIF-67) : m(DHTP) = 2 : 1)] was added. The mixture solution was stirred at room temperature for 20 min and then aged at room temperature for 30 min. The resulting crystals were washed several times with methanol and finally dried at 60 °C under vacuum.

Material characterization

The product was characterized by a Rigaku D/max-ga X-ray diffractometer with Cu Kα radiation (λ = 1.54178 Å). The scan rate was 6° min^{-1} in 2θ ranging from 5° to 40°. Scanning electron microscopy (SEM) was conducted on Hitachi S-8010 with an accelerating voltage of 100 kV. FT-IR spectra were obtained on a Bruker EQUINOX-55 spectrophotometer, and the wavenumber interval was 400–4000 cm^{-1}. Transmission electron microscopy (TEM) images were achieved with FEI Tecnai G2F20. Thermogravimetric analysis (TGA) was performed on a Shimadzu DTG-50 thermal analyzer from room temperature to 800 °C at a heating rate of 10 °C min^{-1}. The BET surface area was determined by N$_2$ adsorption–desorption isotherm measurements at 77 K on an Autosorb iQ Station 1. Samples were outgassed for about 6 h at 150 °C till constant weight. Pore size distribution curves were obtained from the analysis of the desorption portion of the isotherms using the DFT method.

Visible-light-driven water oxidation

The photocatalytic water oxidation experiment was carried out as follows. Briefly, a mixture of MOF catalysts, 10 mL of borate buffer solution (80 mM, pH 8.0–10.0), 1.0 mM [Ru(bpy)$_3$]$^{2+}$, and Na$_2$S$_2$O$_8$ were added to a magnetic stirrer charged reaction vessel and then, the reaction mixture was stirred at room temperature. The gas in the headspace of the reaction vessel was collected and analyzed. To ensure that the air is completely removed, the reaction vessel was sealed with a rubber septum and purged with Ar gas for 5 min. Illumination was performed using a 300 W Xe lamp equipped with a long-pass filter (420 nm cut off). The evolved O$_2$ was analyzed by gas chromatography with a thermal conductivity detector (Shimadzu GC-14B) and a 5 Å molecular sieve column (2 m × 4 mm) using Ar as carrier gas. The catalyst used in the recycle experiment was obtained by amplifying the optimal reaction system by 50 times and recovering the catalyst 5 times accordingly. Then, the catalyst for each recovery was subjected to catalytic performance test under standard conditions.

Conflicts of interest

There are no conflicts to declare.

Acknowledgements

Notes and references

1 W. Kim, B. A. McClure, E. Edri and H. Frei, *Chem. Soc. Rev.*, 2016, **45**, 3221.

2 S. W. Sheehan, J. M. Thomsen, U. Hintermair, R. H. Crabtree, G. W. Brudvig and C. A. Schmuttenmaer, *Nat. Commun.*, 2015, **6**, 6469.

3 D. Jing, L. Guo, L. Zhao, X. Zhang, H. Liu, M. Li, S. Shen, G. Liu, X. Hu, X. Zhang, K. Zhang, L. Ma and P. Guo, *Int. J. Hydrogen Energy*, 2010, **35**, 7087.

4 P. Charvin, A. Stéphane, L. Florent and F. Gilles, *Energy Convers. Manage.*, 2008, **49**, 1547.

5 Y. Wu, Y. Liu, G.-D. Li, X. Zou, X. Lian, D. Wang, L. Sun, T. Asefa and X. Zou, *Nano Energy*, 2017, **35**, 161.

6 M. S. Wangkheimayum, D. Pegram, H. Duan, D. Kalita, P. Simone, L. E. Gary and X. Zhao, *Angew. Chem., Int. Ed.*, 2011, **51**, 1653.

7 H. H. Pham, M.-J. Cheng, H. Frei and L.-W. Wang, *ACS Catal.*, 2016, **6**, 5610.

8 K. Meyer, M. Ranocchiari and J. A. van Bokhoven, *Energy Environ. Sci.*, 2015, **8**, 1923.

9 F. Guo, W. Shi, C. Zhu, H. Li and Z. Kang, *Appl. Catal., B*, 2018, **226**, 412.

10 H. Lv, J. Song, H. Zhu, Y. V. Geletii, J. Bacsa, C. Zhao, T. Lian, D. G. Musaev and C. L. Hill, *J. Catal.*, 2013, **307**, 48.

11 Z. Huang, Z. Luo, Y. V. Geletii, J. W. Vickers, Q. Yin, D. Wu, Y. Hou, Y. Ding, J. Song, D. G. Musaev, C. L. Hill and T. Lian, *J. Am. Chem. Soc.*, 2011, **133**, 2068.

12 S. D. Tilley, M. Cornuz, K. Sivula and M. Grätzel, *Angew. Chem., Int. Ed.*, 2010, **49**, 6405.

13 X. Lin, D. Xu, Y. Xi, R. Zhao, L. Zhao, M. Song, H. Zhai, G. Che and L. Chang, *Colloids Surf., A*, 2017, **513**, 117.

14 X. Lin, Y. Xi, R. Zhao, J. Shi and N. Yan, *RSC Adv.*, 2017, **7**, 53847.

15 X. Lin, D. Xu, S. Jiang, F. Xie, M. Song, H. Zhai, L. Zhao, G. Che and L. Chang, *Catal. Commun.*, 2017, **89**, 96.

16 X. Lin, D. Xu, R. Zhao, Y. Xi, L. Zhao, M. Song, H. Zhai, G. Che and L. Chang, *Sep. Purif. Technol.*, 2017, **178**, 163.

17 N. Shi, W. Cheng, H. Zhou, T. Fan and M. Niederberger, *Chem. Commun.*, 2015, **51**, 1338.

18 M. Wiechen, M. M. Najafpour, S. I. Allakhverdiev and L. Spiccia, *Energy Environ. Sci.*, 2014, **7**, 2203.

19 Z. Wan, Q. Xu, H. Li, Y. Zhang, Y. Ding and J. Wang, *Appl. Catal., B*, 2017, **210**, 67.

20 Q. Xu, H. Li, F. Yue, L. Chi and J. Wang, *New J. Chem.*, 2016, **40**, 3032.

21 D. Wang, J. Guo, D. Hu, Q. Xu, L. Zhang and J. Wang, *ACS Sustainable Chem. Eng.*, 2018, **6**, 8300.

22 S. Yuan, L. Feng, K. Wang, J. Pang, M. Bosch, C. Lollar, Y. Sun, J. Qin, X. Yang, P. Zhang, Q. Wang, L. Zou, Y. Zhang, L. Zhang, Y. Fang, J. Li and H.-C. Zhou, *Adv. Mater.*, 2018, **1704303**, 35.

23 O. K. Farha, I. Eryazici, N. C. Jeong, B. G. Hauser, C. E. Wilmer, A. A. Sarjeant, R. Q. Snurr, S. T. Nguyen, A. Ö. Yazaydın and J. T. Hupp, *J. Am. Chem. Soc.*, 2012, **134**, 15016.

24 T. Kitao, Y. Zhang, S. Kitagawa, B. Wang and T. Uemura, *Chem. Soc. Rev.*, 2017, **46**, 3108.

25 C. D. Wu and M. Zhao, *Adv. Mater.*, 2017, **29**, 1605446.

26 P. Garcia-Garcia, M. Muller and A. Corma, *Chem. Sci.*, 2014, **5**, 2979.

27 K. Maity, K. Bhunia, D. Pradhan and K. Biradha, *ACS Appl. Mater. Interfaces*, 2017, **9**, 37548.

28 J. Wei, Y. Feng, Y. Liu and Y. Ding, *J. Mater. Chem. A*, 2015, **3**, 22300.

29 S. Lin, K. Ravari Alireza, J. Zhu, M. Usov Pavel, M. Cai, R. Ahrenholtz Spencer, Y. Pushkar and J. Morris Amanda, *ChemSusChem*, 2017, **11**, 464.

30 T.-T. Li, J. Qian and Y.-Q. Zheng, *RSC Adv.*, 2016, **6**, 77358.

31 L. Zhang, T. Mi, M. Ziaee, L. Liang and R. Wang, *J. Mater. Chem. A*, 2018, **6**, 1639.

32 G. Xu, Z. Xu, Z. Shi, L. Pei, S. Yan, Z. Gu and Z. Zou, *ChemSusChem*, 2017, **10**, 2897.

33 X. Du, J. Wei, J. Zhao, R. Han and Y. Ding, *Chem. – Asian J.*, 2014, **9**, 2745.

34 K. Koh, A. G. Wong-Foy and A. J. Matzger, *Chem. Commun.*, 2009, 6162.

35 A. Zouitine, A. Ibral, E. Assaid, F. Dujardin and E. Feddi, *Superlattices Microstruct.*, 2017, **109**, 123.

36 L. Liu, H. Ou, K. Hong and L. Wang, *J. Alloys Compd.*, 2018, **749**, 217.

37 Y. Bu and Z. Chen, *Electrochim. Acta*, 2014, **144**, 42.

38 Y. Tang, Y. Hu, L. Song, R. Zong, Z. Gui, Z. Chen and W. Fan, *Polym. Degrad. Stab.*, 2003, **82**, 127.

39 H.-Y. Cho, D.-A. Yang, J. Kim, S.-Y. Jeong and W.-S. Ahn, *Catal. Today*, 2012, **185**, 35.

40 X. Qian, Q. Ren, X. Wu, J. Sun, H. Wu and J. Lei, *ChemistrySelect*, 2018, **3**, 657.

41 J. Wei, Y. Feng, P. Zhou, Y. Liu, J. Xu, R. Xiang, Y. Ding, C. Zhao, L. Fan and C. Hu, *ChemSusChem*, 2015, **8**, 2630.

42 Y. Yamada, K. Yano, D. Hong and S. Fukuzumi, *Phys. Chem. Chem. Phys.*, 2012, **14**, 5753.

43 C. Creutz and N. Sutin, *Inorg. chem.*, 1976, **15**, 496.

44 S.-S. Yi, J.-M. Yan, B.-R. Wulan and Q. Jiang, *J. Mater. Chem. A*, 2017, **5**, 15862.